

ARTICLE



Fundus autofluorescence and optical coherence tomography biomarkers associated with the progression of geographic atrophy secondary to age-related macular degeneration

Patricia T. A. Bui¹, Gregor S. Reiter¹, Maria Fabianska¹, Sebastian M. Waldstein¹, Christoph Grechenig¹, Hrvoje Bogunovic¹, Mustafa Arikani¹ and Ursula Schmidt-Erfurth¹✉

© The Author(s), under exclusive licence to The Royal College of Ophthalmologists 2021

OBJECTIVES: To investigate the impact of qualitatively graded and deep learning quantified imaging biomarkers on growth of geographic atrophy (GA) secondary to age-related macular degeneration.

METHODS: This prospective study included 1062 visits of 181 eyes of 100 patients with GA. Spectral-domain optical coherence tomography (SD-OCT) and fundus autofluorescence (FAF) images were acquired at each visit. Hyperreflective foci (HRF) were quantitatively assessed in SD-OCT volumes using a validated deep learning algorithm. FAF images were graded for FAF patterns, subretinal drusenoid deposits (SDD), GA lesion configuration and atrophy enlargement. Linear mixed models were calculated to investigate associations between all parameters and GA progression.

RESULTS: FAF patterns were significantly associated with GA progression ($p < 0.001$). SDD was associated with faster GA growth ($p = 0.005$). Eyes with higher HRF concentrations showed a trend towards faster GA progression ($p = 0.072$) and revealed a significant impact on GA enlargement in interaction with FAF patterns ($p = 0.01$). The fellow eye status had no significant effect on lesion enlargement ($p > 0.05$). The diffuse-trickling FAF pattern exhibited significantly higher HRF concentrations than any other pattern ($p < 0.001$).

CONCLUSION: Among a wide range of investigated biomarkers, SDD and FAF patterns, particularly in interaction with HRF, significantly impact GA progression. Fully automated quantification of retinal imaging biomarkers such as HRF is both reliable and merited as HRF are indicators of retinal pigment epithelium dysmorphia, a central pathogenetic mechanism in GA. Identifying disease markers using the combination of FAF and SD-OCT is of high prognostic value and facilitates individualized patient management in a clinical setting.

Eye (2022) 36:2013–2019; <https://doi.org/10.1038/s41433-021-01747-z>

INTRODUCTION

Geographic atrophy (GA) is the advanced stage of non-neovascular age-related macular degeneration (AMD) and is responsible for irreversible vision loss in 20% of patients with AMD [1]. More than 8 million people globally were reported to be affected and this number is expected to increase exponentially with the aging population [2]. GA presents as well-demarcated atrophic areas in the macular region with loss of retinal pigment epithelium (RPE), photoreceptors, and the underlying choriocapillaris [3].

GA can be measured through spectral-domain optical coherence tomography (SD-OCT) and fundus autofluorescence (FAF), with high correlations shown between both methods of measurement [4]. Currently, lesion enlargement is the most commonly used anatomical endpoint for the study of GA [5]. Since GA growth rates are known to have high interindividual variability, prediction of an individual's disease progression can be challenging [6]. However, various biomarkers have been identified

to impact GA enlargement. In recent years, the presence of hyperreflective foci (HRF), visualized by SD-OCT, has been studied in GA eyes [7]. While findings of histopathological studies led to several hypotheses regarding their origin, Curcio et al. [8] validated HRF to represent activated RPE cells migrating in an anterior direction within the retina. Their consistent association with progression from earlier AMD stages to GA [9, 10] has garnered considerable scientific interest and demonstrated their role as a relevant disease predictor.

The junctional zone of GA between the healthy and atrophic retina, indicating the area of incipient atrophy, exhibits different patterns of increased FAF, which are highly variable in configuration and intensity [11]. Contrary to a common concept, this hyperautofluorescence is not the result of intracellular lipofuscin accumulation, but rather due to a vertical stacking of RPE cells [12–14]. Faster development of new and enlargement of existing GA with the presence of certain FAF patterns has been described [15].

¹Christian Doppler Laboratory for Ophthalmic Image Analysis, Department of Ophthalmology and Optometry, Medical University of Vienna, Vienna, Austria.

✉email: ursula.schmidt-erfurth@meduniwien.ac.at

Received: 22 January 2021 Revised: 27 July 2021 Accepted: 4 August 2021

Published online: 16 August 2021

Reticular pseudodrusen, also referred to as subretinal drusenoid deposits (SDD), have gained substantial recognition in the context of GA. Although their exact etiology is still unclear, they are believed to represent deposits internal to the RPE, expanding to the overlying photoreceptor layer [16–18]. Prevalence of SDD in GA was reported up to 93% [16], which is considerably higher than in early or intermediate AMD stages. Historically, SDD has been consistently associated with higher conversion risk to GA [16, 19, 20]. Further biomarkers previously described in the context of GA growth include the multilobular lesion configuration, the fellow eye (FE) status, and GA area [6, 21, 22].

GA is a critical unmet medical need given its high incidence and lack of effective treatment. Although the underlying mechanisms leading to GA are not fully understood yet, the advent of multimodal imaging has considerably improved our understanding of its pathophysiology. This study was performed to simultaneously investigate a wide range of quantitative and qualitative biomarkers assessed using artificial intelligence (AI) and the combination of FAF and SD-OCT and their impact on GA growth including HRF, a relatively recent biomarker that has not been widely explored yet, in a large cohort of patients with a narrow follow-up exhibiting natural disease progression.

MATERIALS AND METHODS

Study design, inclusion, and exclusion criteria

This prospective study was conducted at the Department of Ophthalmology at the Medical University of Vienna, Austria. Patients aged 50 years or older who were diagnosed with GA secondary to AMD and followed for a minimum of 12 months were included. Study visits occurred every 3 months. Eyes were excluded if there was a history of other ocular diseases that would confound retinal assessment, particularly neovascular AMD, if macular atrophy was due to other retinal conditions, and if there were coalescent lesions of peripapillary atrophy and GA. Furthermore, FAF images with insufficient quality regarding contrast and sharpness, thus not allowing for accurate assessment of atrophy size and features, were not analyzed either.

The presented study was approved by the Ethics Committee of the Medical University of Vienna. The research was performed in compliance with the tenets of the Declaration of Helsinki and Good Clinical Practice. Written informed consent was given by all patients before any study-specific procedure.

FAF and SD-OCT imaging

At each visit, FAF and SD-OCT scans were recorded, using Spectralis HRA + OCT (Heidelberg Engineering, Heidelberg, Germany). All FAF images encompassed the macular area including at least a portion of the optic disk

and were collected according to the following protocol: excitation wavelength 488 nm, barrier filter at 500 nm, 30° × 30° field of view, image resolution of 768 × 768 and 1536 × 1536 pixels and a mean of 20 single images. The SD-OCT scans were acquired with a field of view of 20° × 20° and a resolution of 1024 × 49 (A-scans × B-scans). In order to enhance the signal-to-noise ratio, the automatic retinal tracking (ART) mode was applied for the generation of mean images of 9 SD-OCT single frames. All scans were exported for grading of GA area, FAF patterns, SDD, lesion configuration in FAF, and HRF concentration in SD-OCT.

FAF and SD-OCT grading

FAF scans were imported into validated image analysis software (OCTAVO, Vienna Reading Center, Vienna, Austria). For each visit, the total size of GA was measured manually in all FAF images by delineating atrophic areas—defined as well-demarcated areas with a very low or extinguished degree of autofluorescence [6]. Peripapillary atrophy was not included in the measurements. The GA area was transformed using the previously established square root (sqrt) transformation [23]. The difference of sqrt GA areas between consecutive visits was calculated and extrapolated to yearly growth rates (mm/y).

Further, all FAF scans were graded for the presence of increased autofluorescence and classified into six categories of FAF patterns based on the definitions of the FAM study [15] for each visit. All inconclusive cases were additionally reviewed by a second-grader. Furthermore, FAF scans of the baseline visits were evaluated for the presence of a multilobular lesion configuration, defined as the coalescence of multiple lobules into a single atrophy patch. Of note, the term multilobular was defined differently to multifocal as the latter did not show coalescence of atrophic areas. Moreover, for each visit, FAF images were assessed for the presence or absence of SDD, defined as a net-like pattern of spot-like hypoautofluorescent lesions against a background of increased autofluorescence [18]. A random subset of at least 10% of all scans was additionally graded for SDD by a second grader in order to assess inter-reader agreement.

HRF were segmented automatically in all SD-OCT volumes using a validated deep learning algorithm [24]. The difference in magnification between the FAF image and the SD-OCT volume was corrected by spatially registering the FAF image and the corresponding near-infrared reflectance (NIR) image, thus mapping it into a coordinate system of SD-OCT. This method accounts for comparable areas and volumes (i.e., GA annotated in FAF, HRF annotated in SD-OCT) (see Fig. 1). For each visit, the concentration of HRF was measured in the following way: the en-face SD-OCT image was created by marking all A-scans that contain an HRF. The number of such HRF-containing A-scans was then divided by the number of A-scans outside of GA. This resulted in a dimensionless unit denoting the proportion of an area outside GA covered by HRF.

Further variables included in the analysis were patient age (expressed for each visit), gender, laterality (right vs. left eye), and the FE status (intermediate AMD [iAMD], macular neovascularization [MNV], GA or MNV + GA simultaneously present).

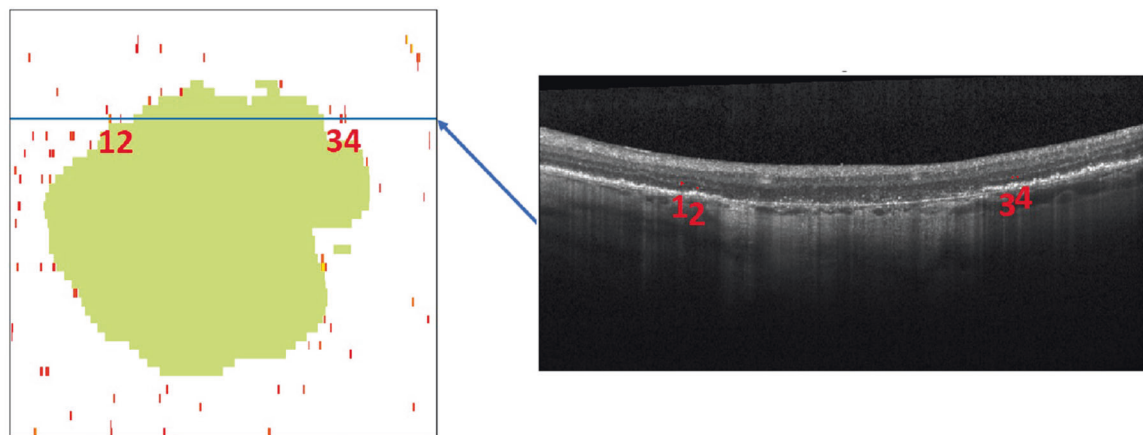


Fig. 1 Illustration of the registration procedure. The left image shows the projection of geographic atrophy (green), extracted from fundus autofluorescence, on the optical coherence tomography C-scan viewed from above. The right image shows the marked B-scan (blue line). The numbers 1–4 indicate the same hyperreflective foci in both images.

Table 1. Summary of demographic and clinical characteristics collected from 181 study eyes.

Data type	Data
Baseline age (years), mean (SD)	75.8 (7.4)
Female sex, no. (% eyes)	64 (65.2)
Follow-up period (months), median (IQR)	30 (24–36)
<i>Fellow eye, no. (%)</i>	
iAMD	2 (1.1)
GA	174 (94.1)
MNV	6 (3.2)
GA + MNV	3 (1.6)
<i>Baseline SDD, no. (%)</i>	
Yes	110 (60.8)
No	61 (33.7)
Remaining ^a	10 (5.5)
<i>Baseline FAF patterns, no. (%)</i>	
None	11 (6.1)
Focal	33 (18.2)
(Patchy) ^b	(1 [0.6])
Banded	34 (18.8)
Diffuse	84 (46.4)
Diffuse-trickling	11 (6.1)
Remaining ^c	7 (3.9)
<i>Baseline multilobular configuration, no. (%)</i>	
Yes	43 (23.8)
No	115 (63.5)
Remaining ^d	23 (12.7)
Sqrt GA area (mm), mean (95% CI)	2.72 (1.56–3.87)
Sqrt GA growth rate (mm/y), mean (95% CI)	0.22 (0.08–0.37)
HRF concentration, mean (95% CI)	0.18 (0.11–0.24)

iAMD intermediate age-related macular degeneration, GA geographic atrophy, MNV macular neovascularization, FAF fundus autofluorescence, SDD subretinal drusenoid deposits, sqrt square root, HRF hyperreflective foci.

^aThese eyes were not gradable due to insufficient image quality.

^bDue to the low frequency the single eye was not considered in the statistical model.

^cThese eyes were not gradable due to insufficient image quality or the absence of a predominant FAF pattern.

^dThese eyes were graded inconclusive as the coalescence of the individual lobules was only partial.

Statistical analysis

As data from all 1062 visits were included in the statistical analysis, possible changes of FAF patterns, SDD and HRF concentrations during the disease course were accounted for. To examine parameter interactions, exploratory linear mixed models were calculated first. Because for some patients both eyes were included in the study, a patient-specific random intercept was specified. Due to a variable number of visits per eye, a second eye-specific random intercept was specified, which was nested in the random effect for the patient. In total, five exploratory models were calculated with different dependent variables: HRF, FAF patterns, multilobularity, SDD, and sqrt GA area. Significant associations were included as interactions in the subsequent GA growth model. The statistical significance level was set at $\alpha = 0.05$.

A linear mixed model was then computed with sqrt GA growth (mm/y) as the dependent variable and the two random effects for the patient and eye. The presence of SDD, FAF patterns, HRF concentration, GA configuration (multilobularity), sqrt GA area, age, gender, laterality, and

FE status (intermediate AMD, MNV, GA, mixed MNV + GA) were included as fixed factors. The following significant interactions from the exploratory models were included in the model: HRF*SDD ($p = 0.008$), HRF*FAF patterns ($p < 0.001$), HRF*age(visit) ($p < 0.001$), SDD*gender ($p < 0.001$), sqrt GA area*age(visit) ($p < 0.001$), sqrt GA area*FAF patterns ($p < 0.001$), FAF patterns*multilobularity ($p = 0.003$). The best model fit was chosen using the corrected Akaike information criterion (cAIC). The least significant factor was removed from the model until no improvement in the model performance was achieved. Furthermore, Kappa coefficients were used to assess the inter-reader reproducibility of the SDD grading. Post-hoc pairwise comparison was adjusted for multiplicity through Bonferroni correction. Residuals of the final model were checked for normal distribution using histograms. All statistical analyses were carried out with the software Prism version 8 (GraphPad Software LLC, San Diego, USA) and SPSS version 26 (IBM, Armonk, USA).

RESULTS

A total number of 1045 FAF and 1062 SD-OCT volumes were analyzed in this study. Overall, 1062 visits of 181 eyes of 100 patients were included. Sixty-four (65.2%) eyes were from female participants. The mean patient age at the baseline visit was 75.8 ± 7.4 years.

Eighty-seven patients had bilateral GA. Two eyes (11 visits) had iAMD, 6 eyes (39 visits) had MNV, and 3 eyes (17 visits) presented with mixed late (GA + MNV) AMD in the FE. One FE converted from iAMD to MNV and 3 eyes developed MNV additionally to GA in this study. These four eyes were counted twice for the prior descriptive analysis for the number of FE, but not for the visits. The visit level-wise status for each FE was considered in the statistical model.

Follow-up duration ranged from 12 to 72 months with a median of 30 (interquartile range (IQR), 24–36) months. The mean sqrt GA area was 2.7 (95% confidence interval (CI), 1.56–3.87) mm. The GA lesions enlarged by a mean of 0.22 (95% CI, 0.08–0.37) mm/y. The mean HRF concentration was 0.18 (95% CI, 0.11–0.24). Table 1 reports detailed distributions of demographic and clinical characteristics. Cohen's Kappa used to assess inter-reader reproducibility of the SDD grading resulted in 0.81.

The exploratory models revealed the diffuse-trickling pattern to exhibit significantly higher HRF concentrations than any other pattern, with a mean of 0.035 (95% CI, 0.025–0.044; $p < 0.001$). Pairwise comparison is shown in Fig. 2 (top left). SDD was significantly associated with the female gender ($p < 0.001$).

In order to achieve the best fit model for GA progression based on cAIC, the following least significant parameters and interactions were removed: multilobular GA configuration, gender, laterality, HRF*SDD, HRF*age, SDD*gender, sqrt GA area*FAF patterns and FAF patterns*multilobularity. The final GA growth model included FAF patterns, HRF concentration, SDD, FE status, and the interactions HRF*FAF patterns and age(visit)*sqrt GA area. Residuals from the final model were normally distributed.

Temporally, sqrt GA growth was significantly associated with FAF patterns ($p < 0.001$), with the diffuse-trickling pattern showing significantly higher mean sqrt GA growth of 0.65 mm/y (95% CI, 0.43–0.86; $p < 0.001$) than any other pattern. Pairwise comparison is presented in Fig. 2 (top right). SDD was positively associated with sqrt GA growth ($p = 0.005$; Fig. 2, bottom). In the final model, a significant association was also found for the interaction HRF*FAF patterns ($p = 0.01$). Age(visit)*sqrt GA area was negatively associated with sqrt GA growth ($p = 0.001$). Eyes with higher HRF concentrations showed a trend towards faster GA progression, which did not reach significance as an individual factor ($p = 0.072$). No significant association was found for FE status ($p = 0.13$). Estimates and detailed p-values (calculated using T-statistic) of all parameters included in the growth model are reported in Table 2. Lastly, Table 3 shows p-values (calculated using F-statistic) of all parameters included in the final best fit model for GA growth.

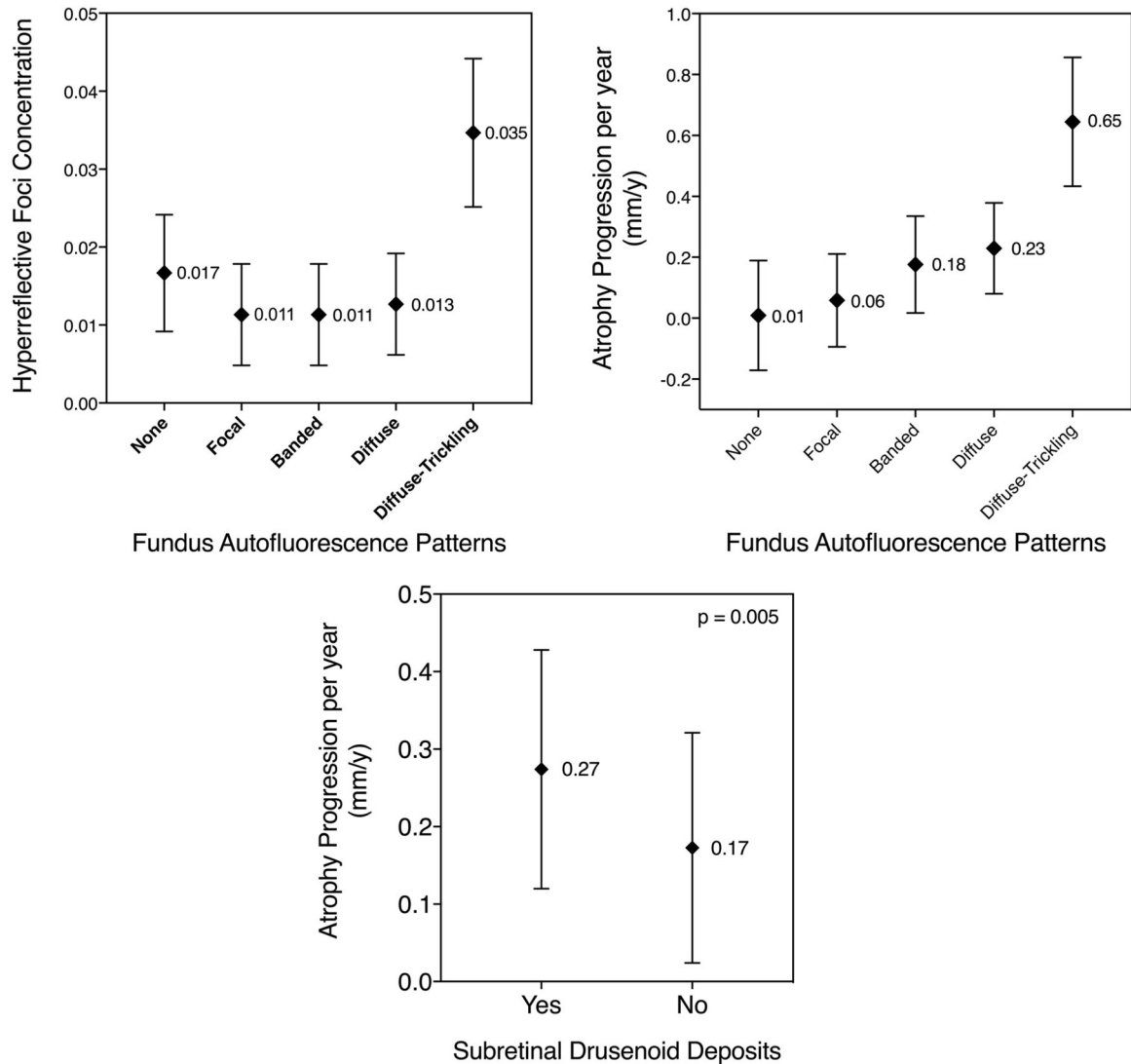


Fig. 2 Pairwise comparison of mean and 95% confidence intervals. *Top left:* comparison of hyperreflective foci (HRF) concentrations between fundus autofluorescence (FAF) patterns. Statistically significant differences in HRF concentrations were found for diffuse-trickling vs. any other pattern (all $p < 0.001$), none vs. focal ($p = 0.03$), and none vs. banded ($p = 0.03$). All other pairwise comparisons were not significant ($p > 0.05$). Adjustment for multiplicity through Bonferroni correction was performed. *Top right:* comparison of geographic atrophy (GA) progression (mm/y) between FAF patterns. Statistically significant differences in growth rates were found for diffuse-trickling vs. any other pattern (all $p < 0.001$), none vs. diffuse ($p = 0.002$), and focal vs. diffuse ($p = 0.002$). All other pairwise comparisons were not significant ($p > 0.05$). Adjustment for multiplicity through Bonferroni correction was performed. *Bottom:* comparison of GA progression (mm/y) in eyes with and without subretinal drusenoid deposits. The difference between the two groups was statistically significant ($p = 0.005$).

DISCUSSION

In this paper, we studied FAF images and SD-OCT volumes in a large set of visits of eyes with GA secondary to AMD. The main objective was to investigate the role of a wide range of quantitative and qualitative biomarkers in atrophy progression. Current studies most commonly focus on the enlargement of GA lesions as a structural endpoint, which is atrophy growth expressed as change in size per year [5]. However, the dependency of progression rate on the baseline lesion size has been described, with larger atrophic lesions at baseline growing faster [6]. In order to eliminate this confounding effect, we performed the previously established sqrt transformation [23], which was shown to remove the correlation between baseline atrophy size and growth rate and we thus reported GA progression as mm growth per year.

The role of increased FAF both in the junctional zone and outside of GA has been widely studied in the last decade.

Histological studies demonstrated increased FAF to be caused by RPE dysmorphia and vertically superimposed RPE cells. Thus, hyperautofluorescence is an indicator of the disorganization of cellular layers [12–14, 25]. This study showed that qualitatively measured FAF patterns have an impact on GA progression ($p < 0.001$). This is also supported by Shen et al., who have analyzed the GA radius growth rates for each pattern and demonstrated their independence from baseline size within each group but significantly differing growth rates between the groups, indicating an assertive predictive role of FAF phenotypes in GA growth [26].

Ho et al. were the first to describe HRF in OCT images of eyes with early and intermediate AMD, visualized as discreet hyperreflective and highly backscattering lesions within the retinal layers [27]. Some authors ascribed them to activated microglial immune cells migrating to the subretinal space and interfering with RPE cell function [28], however, the most widely accepted concept at present appears to be that by Curcio et al. who confirmed HRF in

Table 2. Estimates (growth of geographic atrophy [GA] per year in mm) for all parameters included in the best fit model for GA progression.

Parameter	Estimate	P-value	Lower 95% CI	Upper 95% CI
FAF Pattern (focal) ^a	0.243	0.019*	0.04	0.446
FAF Pattern (banded) ^a	0.319	0.004*	0.104	0.534
FAF Pattern (diffuse) ^a	0.4	<0.001*	0.209	0.591
FAF Pattern (diffuse-trickling) ^a	0.89	<0.001*	0.611	1.169
HRF concentration	13.336	0.01	5.465	21.208
HRF*FAF Pattern (focal) ^a	-13.258	0.008*	-23.001	-3.511
HRF*FAF Pattern (banded) ^a	-10.412	0.08	-22.089	1.265
HRF*FAF Pattern (diffuse) ^a	-12.285	0.01*	-21.534	-3.035
HRF*FAF Pattern (diffuse-trickling) ^a	-17.458	<0.001*	-26.881	-8.036
SDD presence (yes)	0.102	0.005*	0.031	0.173
Age(visit)*sqrt GA area	-0.001	0.001*	-0.001	0
Fellow eye (MNV) ^b	-0.112	0.678	-0.641	0.417
Fellow eye (GA) ^b	0.096	0.701	-0.396	0.589
Fellow eye (GA + MNV) ^b	0.001	0.996	-0.535	0.538

FAF fundus autofluorescence, HRF hyperreflective foci, MNV macular neovascularization, GA geographic atrophy, iAMD intermediate age-related macular degeneration, SDD subretinal drusenoid deposits, sqrt square root, CI confidence interval.

*Statistical significance $p \leq 0.05$.

^aCompared to FAF Pattern (none).

^bCompared to iAMD.

Table 3. P-values of all parameters included in the final best fit model for geographic atrophy progression.

Parameter	P-value
FAF patterns	<0.001*
HRF	0.072
HRF*FAF patterns	0.01*
FE status	0.134
SDD presence (yes)	0.005*
Age(visit)*sqrt GA area	0.001*

FAF fundus autofluorescence, HRF hyperreflective foci, SDD subretinal drusenoid deposits, FE fellow eye, GA geographic atrophy.

*Statistical significance $p \leq 0.05$.

AMD to represent activated RPE cells migrating in an anterior direction in SD-OCT scans [8]. Various studies have demonstrated HRF to be a precursor to new atrophy onset [8–10, 29–33]. The concept of HRF preceding atrophy seems plausible considering that migrating RPE cells may express a dysregulated and unfavorable microenvironment within the RPE cell layer [30]. However, it is uncertain which role HRF plays in the growth of existing GA. Given the recent advances in AI, it has become possible to reliably grade and analyze larger data sets fully automatically [34]. In this analysis, HRF was segmented by a state-of-the-art deep learning algorithm. Although we only found a trend between HRF and faster global GA growth ($p = 0.072$), our results indicated that eyes with higher HRF concentrations are significantly associated with GA enlargement in interaction with FAF patterns ($p = 0.01$).

What is more, our exploratory models revealed HRF to be significantly linked to FAF patterns ($p < 0.001$), specifically the diffuse-trickling pattern to exhibit up to three times higher concentrations of HRF than any other patterns ($p < 0.001$). Given their common origin RPE dysmorphia and disintegration of the RPE layer, with HRF representing activated migrating RPE cells [8] and elevated FAF indicating vertically stacked RPE cells [12, 13, 25], it seems very plausible for diffuse-trickling eyes, a

phenotype with more extensive alterations in FAF, to feature higher HRF amounts.

The presence of SDD has been consistently linked to faster conversion to GA and CNV in the last decade [19, 20]. Our study, however, demonstrated that SDD also accelerates the growth of existing GA ($p = 0.005$). The calculated estimate indicates a faster growth by 0.1 mm per mm atrophy growth per year (10%) if SDD is present. A recent study from Reiter et al. [35], also confirmed SDD to be associated with faster GA growth. Furthermore, Xu et al. even proposed SDD to develop into multilobular GA, as the authors detected significant spatial correlations [16]. In conclusion, our findings add to the growing recognition of SDD as an important biomarker for the progression of existing GA.

Interestingly, the interaction age(visit)*sqrt GA area was significantly negatively associated with sqrt GA growth ($p = 0.001$, estimate = -0.001), indicating a decelerating effect of larger lesions conjoined with older age on GA enlargement. Similarly, Monés et al. detected a negative correlation between sqrt transformed baseline atrophy area and GA growth rate [22]. This may be explained by the tendency of smaller lesions to have an irregular and multifocal shape, whereas larger lesions often coalesce and take a more circular shape. The increase in circularity often equals a decrease in lesion perimeter, which in turn may signify less contact between atrophic RPE cells and adjacent healthy cells, thus decelerating lateral atrophy spread [22]. Furthermore, Shen et al. described varying GA radius growth rates dependent on topographic zones, with decreasing growth in areas beyond the macular region i.e., larger lesions [3]. Therefore, varying baseline areas must be accounted for in the further analysis and sqrt transformation appears to be a valid tool to evade non-linear GA growth.

The FE status has been known to impact GA progression, with accelerated enlargement if the FE has GA and/or MNV versus iAMD [21]. However, we revealed no faster growth with advanced AMD present in the FE ($p = 0.13$). This could be explained by the distribution of our data, as FE status was predominantly GA for most of the patients, hence the effect of FE might have been altered by this proportion.

Some limitations of this study should be acknowledged. We investigated the impact of presence or absence of SDD on GA

growth, however, we did not quantify nor topographically localize SDD. This could nonetheless be of value as it may enhance our understanding of their nature. Identification and quantification of SDD may be most efficiently performed using AI in future analyses [36]. Moreover, there are certain disadvantages to FAF including the impossibility of obtaining depth information and the limited assessment of foveal atrophy [37]. Most notably, interpretation of FAF images can be challenging considering the lack of absolute quantification of the local and background signals [38]. The classification of a pixel as hypo- or hyperautofluorescent is based on a relative comparison. A quantitative approach that measures the intensities of the FAF greyscale and a consensus on a threshold for elevated and reduced FAF are needed in order to reliably assess retinal diseases [38].

The main strengths of this study include the prospective nature of our study along with a standardized imaging protocol and steady follow-up intervals, our narrow range of exclusion criteria allowing for good transferability to the general population, and the rigorous standardized image analysis. Importantly, although some of the investigated parameters and their individual effects on GA growth have been reported before, we examined the simultaneous impact of a wide and variable range of biomarkers on atrophy enlargement, providing a reliable progression model for GA. Moreover, we included the significant parameter interactions from the exploratory models in our final growth model, which allowed for high model performance. Furthermore, we used state-of-the-art deep learning algorithms allowing for a reliable and detailed quantitative assessment of HRF. Finally, we examined a large cohort of patients with a narrow follow-up and thus a substantial number of visits, exhibiting natural disease progression.

In conclusion, we found the presence of SDD and distinct FAF patterns to independently impact GA growth to the highest degree among a wide range of investigated biomarkers. Also, we demonstrated eyes with higher HRF concentrations to be significantly associated with GA enlargement in interaction with FAF patterns. Furthermore, we detected the diffuse-trickling phenotype to exhibit higher HRF concentrations than any other FAF pattern. Identifying such disease markers using the combination of FAF and SD-OCT and precisely quantifying them using AI facilitates individualized patient management and enables more streamlined treatment trials as well as deepens our understanding of the complex multifactorial nature of non-neovascular AMD.

Summary

What was known before

- Currently, lesion enlargement is the most commonly used anatomical endpoint for the study of geographic atrophy (GA). Various biomarkers assessed using fundus autofluorescence (FAF) and spectral-domain optical coherence tomography have been associated with GA progression, including subretinal drusenoid deposits, FAF patterns, multilobular atrophy, GA area.
- Hyperreflective foci (HRF) have been linked to progression from earlier AMD stages to GA.

What this study adds

- Although some of the investigated biomarkers and their individual effects on GA progression have been reported before, this study examined the simultaneous impact of a wide and variable range of biomarkers on atrophy progression, providing a reliable growth model for GA.
- State-of-the-art deep learning algorithms were used allowing for a reliable and detailed quantitative assessment of HRF, a

relatively recent biomarker, that has not been widely explored yet, particularly in the context of enlargement of existing GA.

REFERENCES

1. Sunness JS. The natural history of geographic atrophy, the advanced atrophic form of age-related macular degeneration. *Mol Vis*. 1999;5:25.
2. Schmitz-Valckenberg S, Sahel JA, Danis R, Fleckenstein M, Jaffe GJ, Wolf S, et al. Natural history of geographic atrophy progression secondary to age-related macular degeneration (geographic atrophy progression study). *Ophthalmology*. 2016;123:361–8.
3. Shen LL, Sun M, Khetpal S, Grossetta Nardini HK, Del Priore LV. Topographic variation of the growth rate of geographic atrophy in nonexudative age-related macular degeneration: a systematic review and meta-analysis. *Investig Ophthalmol Vis Sci*. 2020;61:2.
4. Simader C, Sayegh RG, Montuoro A, Azhary M, Koth AL, Baratsits M, et al. A longitudinal comparison of spectral-domain optical coherence tomography and fundus autofluorescence in geographic atrophy. *Am J Ophthalmol*. 2014;158:557–66.e1.
5. Schaal KB, Rosenfeld PJ, Gregori G, Yehoshua Z, Feuer WJ. Anatomic clinical trial endpoints for nonexudative age-related macular degeneration. *Ophthalmology*. 2016;123:1060–79.
6. Fleckenstein M, Mitchell P, Freund KB, Sadda S, Holz FG, Brittain C, et al. The progression of geographic atrophy secondary to age-related macular degeneration. *Ophthalmology*. 2018;125:369–90.
7. Schmidt-Erfurth U, Bogunovic H, Grechenig C, Bui P, Fabianska M, Waldstein S, et al. Role of deep learning-quantified hyperreflective foci for the prediction of geographic atrophy progression. *Am J Ophthalmol*. 2020;216:257–70.
8. Curcio CA, Zanzottera EC, Ach T, Balaratnasingam C, Freund KB. Activated retinal pigment epithelium, an optical coherence tomography biomarker for progression in age-related macular degeneration. *Investig Ophthalmol Vis Sci*. 2017;58:Bio211–bio26.
9. Christenbury JG, Folgar FA, O'Connell RV, Chiu SJ, Farsi S, Toth CA. Progression of intermediate age-related macular degeneration with proliferation and inner retinal migration of hyperreflective foci. *Ophthalmology*. 2013;120:1038–45.
10. Nassisi M, Fan W, Shi Y, Lei J, Borrelli E, Ip M, et al. Quantity of intraretinal hyperreflective foci in patients with intermediate age-related macular degeneration correlates with 1-year progression. *Investig Ophthalmol Vis Sci*. 2018;59:3431–9.
11. Holz FG, Bellmann C, Margaritidis M, Schutt F, Otto TP, Volcker HE. Patterns of increased in vivo fundus autofluorescence in the junctional zone of geographic atrophy of the retinal pigment epithelium associated with age-related macular degeneration. *Graefes Arch Clin Exp Ophthalmol*. 1999;237:145–52.
12. Rudolf M, Vogt SD, Curcio CA, Huisingh C, McGwin G Jr, Wagner A, et al. Histologic basis of variations in retinal pigment epithelium autofluorescence in eyes with geographic atrophy. *Ophthalmology*. 2013;120:821–8.
13. Zanzottera EC, Ach T, Huisingh C, Messinger JD, Freund KB, Curcio CA. Visualizing retinal pigment epithelium phenotypes in the transition to atrophy in neovascular age-related macular degeneration. *Retina*. 2016;36:S26–s39. Suppl 1(Suppl 1)
14. Reiter GS, Told R, Baumann L, Sacu S, Schmidt-Erfurth U, Pollreis A, et al. Investigating a Growth prediction model in advanced age-related macular degeneration with solitary geographic atrophy using quantitative autofluorescence. *Retina*. 2020;40:1657–64.
15. Holz FG, Bindewald-Wittich A, Fleckenstein M, Dreyhaupt J, Scholl HP, Schmitz-Valckenberg S. Progression of geographic atrophy and impact of fundus autofluorescence patterns in age-related macular degeneration. *Am J Ophthalmol*. 2007;143:463–72.
16. Xu L, Blonska AM, Pumariega NM, Bearely S, Sohrab MA, Hageman GS, et al. Reticular macular disease is associated with multilobular geographic atrophy in age-related macular degeneration. *Retina*. 2013;33:1850–62.
17. Zweifel SA, Spaide RF, Curcio CA, Malek G, Imamura Y. Reticular pseudodrusen are subretinal drusenoid deposits. *Ophthalmology*. 2010;117:303–12.e1.
18. Wightman AJ, Guymmer RH. Reticular pseudodrusen: current understanding. *Clin Exp Optom*. 2019;102:455–62.
19. Marsiglia M, Boddu S, Bearely S, Xu L, Breaux BE Jr, Freund KB, et al. Association between geographic atrophy progression and reticular pseudodrusen in eyes with dry age-related macular degeneration. *Investig Ophthalmol Vis Sci*. 2013;54:7362–9.
20. Pumariega NM, Smith RT, Sohrab MA, Letien V, Souied EH. A prospective study of reticular macular disease. *Ophthalmology*. 2011;118:1619–25.
21. Shen LL, Liu F, Grossetta Nardini HK, Del Priore LV. Fellow eye status is a biomarker for the progression rate of geographic atrophy: a systematic review and meta-analysis. *Ophthalmol Retina*. 2019;3:305–15.

22. Monés J, Biarnés M. The rate of progression of geographic atrophy decreases with increasing baseline lesion size even after the square root transformation. *Transl Vis Sci Technol*. 2018;7:40.
23. Yehoshua Z, Rosenfeld PJ, Gregori G, Feuer WJ, Falcão M, Lujan BJ, et al. Progression of geographic atrophy in age-related macular degeneration imaged with spectral domain optical coherence tomography. *Ophthalmology* 2011;118:679–86.
24. Schlegl T, Bogunovic H, Klmscha S, Seeböck P, Sadeghipour A, Gerendas B, et al. Fully automated segmentation of hyperreflective foci in optical coherence tomography images. 2018;arXiv:18050327.
25. Ach T, Huisingh C, McGwin G Jr., Messinger JD, Zhang T, Bentley MJ, et al. Quantitative autofluorescence and cell density maps of the human retinal pigment epithelium. *Investig Ophthalmol Vis Sci*. 2014;55:4832–41.
26. Shen LL, Liu F, Nardini HG, Del Priore LV. Reclassification of fundus autofluorescence patterns surrounding geographic atrophy based on progression rate: a systematic review and meta-analysis. *Retina*. 2019;39:1829–39.
27. Ho J, Witkin AJ, Liu J, Chen Y, Fujimoto JG, Schuman JS, et al. Documentation of intraretinal retinal pigment epithelium migration via high-speed ultrahigh-resolution optical coherence tomography. *Ophthalmology* 2011;118:687–93.
28. Ma W, Zhao L, Fontainhas AM, Fariss RN, Wong WT. Microglia in the mouse retina alter the structure and function of retinal pigmented epithelial cells: a potential cellular interaction relevant to AMD. *PLoS ONE*. 2009;4:e7945.
29. Sleiman K, Veerappan M, Winter KP, McCall MN, Yiu G, Farsiu S, et al. Optical coherence tomography predictors of risk for progression to non-neovascular atrophic age-related macular degeneration. *Ophthalmology* 2017;124:1764–77.
30. Lei J, Balasubramanian S, Abdelfattah NS, Nittala MG, Sadda SR. Proposal of a simple optical coherence tomography-based scoring system for progression of age-related macular degeneration. *Graefes Arch Clin Exp Ophthalmol*. 2017;255:1551–8.
31. Schmidt-Erfurth U, Waldstein SM, Klmscha S, Sadeghipour A, Hu X, Gerendas BS, et al. Prediction of individual disease conversion in early AMD using artificial intelligence. *Investig Ophthalmol Vis Sci*. 2018;59:3199–208.
32. Balaratnasingam C, Yannuzzi LA, Curcio CA, Morgan WH, Querques G, Capuano V, et al. Associations between retinal pigment epithelium and drusen volume changes during the lifecycle of large drusenoid pigment epithelial detachments. *Investig Ophthalmol Vis Sci*. 2016;57:5479–89.
33. Ouyang Y, Heussen FM, Hariri A, Keane PA, Sadda SR. Optical coherence tomography-based observation of the natural history of drusenoid lesion in eyes with dry age-related macular degeneration. *Ophthalmology*. 2013;120:2656–65.
34. Liefers BCJ, González-Gonzalo C, Verzijden T, Wang JJ, Joachim N, Mitchell PHC, et al. A deep learning model for segmentation of geographic atrophy to study its long-term natural history. *Ophthalmology*. 2020;127:1086–96.
35. Reiter GS, Told R, Schranz M, Baumann L, Mylonas G, Sacu S, et al. Subretinal drusenoid deposits and photoreceptor loss detecting global and local progression of geographic atrophy by SD-OCT imaging. *Investig Ophthalmol Vis Sci*. 2020;61:11.
36. van Grinsven MJ, Buitendijk GH, Brussee C, van Ginneken B, Hoyng CB, Theelen T, et al. Automatic identification of reticular pseudodrusen using multimodal retinal image analysis. *Investig Ophthalmol Vis Sci*. 2015;56:633–9.
37. Sadda SR, Chakravarthy U, Birch DG, Staurengi G, Henry EC, Brittain C. Clinical endpoints for the study of geographic atrophy secondary to age-related macular degeneration. *Retina*. 2016;36:1806–22.
38. Frampton GK, Kalita N, Payne L, Colquitt JL, Loveman E, Downes SM, et al. Fundus autofluorescence imaging: systematic review of test accuracy for the diagnosis and monitoring of retinal conditions. *Eye*. 2017;31:995–1007.

ACKNOWLEDGEMENTS

The authors have not declared a specific grant for this research from any funding agency in the public, commercial or not-for-profit sectors.

AUTHOR CONTRIBUTIONS

US-E, SMW, and PTAB designed the research; GSR, CG, HB, and PTAB acquired and analyzed the data; MF and MA provided technical support; US-E, GSR, CG, HB, and SMW contributed to critical revision of the article; US-E provided resources, supervised the project and gave final approval for submitting; SMW provided resources and supervised the project; PTAB wrote the article.

COMPETING INTERESTS

US-E serves as a consultant to Genentech, Heidelberg Engineering, Kodiak, Novartis, RetInSight, and Roche—all unrelated to this study. SMW serves as a consultant to Novartis and receives research support from Bayer and Genentech—all unrelated to this study. PTAB, GSR, MF, CG, HB, and MA declare no conflict of interests.

ADDITIONAL INFORMATION

Correspondence and requests for materials should be addressed to U.S-E.

Reprints and permission information is available at <http://www.nature.com/reprints>

Publisher's note Springer Nature remains neutral with regard to jurisdictional claims in published maps and institutional affiliations.